

7A.6 Detection of Thermohaline Structure and Meridional Overturning Circulation Above and Below the Ocean Surface

Peter C. Chu¹⁾, Charles Sun²⁾, and Chenwu Fan¹⁾

¹⁾ Naval Ocean Analysis and Prediction Laboratory
Department of Oceanography
Naval Postgraduate School, Monterey, California
²⁾ NOAA/NODC, Silver Spring, Maryland

1. Introduction

Ocean temperature, salinity, and currents available at the present time do not have sufficient resolution to describe the variability in Meridional Overturning Circulation (MOC). We use our unique data access, our strong experience in analysis of sparse and noisy ocean data, and our data system already in place at NOAA/NODC and the Naval Postgraduate School (NPS), to produce and distribute three dimensional temperature, salinity, and velocity fields using the Global Temperature-Salinity Profile Program (GTSP) and Argo profile and track data together with the Navy's Master Observational Oceanographic Data Set (MOODS), at spatial resolution equal and higher than the standard product ($1^\circ \times 1^\circ$). The temporal and spatial resolution was improved by merging with data from the Ocean Surface Current Analyses – Real Time (OSCAR) derived from satellite altimeter and scatterometer. Close partnership between NPS and NOAA/NODC shows the impact of the temporally varying temperature, salinity, and velocity data on operational monitoring of MOC, thermohaline structure, and associated rapid climatic change. More flexible and user-driven data processing and distributing system will be implemented, to optimize data use by both the scientific and operational communities. With the reanalyzed three dimensional ocean fields for two decades (1990-2008), we identified temporal and spatial variability of MOC and thermohaline structure.

¹⁾ **Corresponding author address: Peter C. Chu, Naval Postgraduate School, Monterey, CA 93943, email: pccchu@nps.edu**

Since rapid changes in MOC could have implications for regional changes of climate, correlation analysis between our reanalyzed datasets (3D ocean fields) and the surface atmospheric data (such as NCEP reanalyzed wind stress, air-ocean heat and moisture fluxes) will improve understanding of the physical mechanisms behind fluctuations in the thermohaline structure and MOC.

2. Atlantic MOC

A major feature of the basin-scale circulation in the North Atlantic is the existence of the robust AMOC. Driven largely by the deep-water formation in the Labrador and Nordic seas, the AMOC is the main mechanism for northward heat transport in the Atlantic Ocean. Cross-equatorial heat flux associated with the AMOC occurs through northward transport of warm surface waters from the southern Atlantic Ocean and southward transport of cold deep waters by the deep western boundary current (DWBC). Changes in the Labrador Cold water formation affect the MOC and subsequently the sea surface temperature (SST) in the tropics (Curry and McCartney, 1996; Broecker, 1997; Curry et al., 1998).

During the World Ocean Circulation Experiment (WOCE) 1990-1998, nine realizations conducted along "48°N" section (from the English Channel to the Grand Banks of Newfoundland) showed significant inter-annual variability in climate-relevant key parameters such as heat and fresh water transports. With a phase lag of one to two years, the transport is almost linearly correlated to the changes of the dominant mode of low-frequency atmospheric variability in the North Atlantic, the North Atlantic Oscillation (NAO) [Bersh, (2002)]. Frankignoul et al. (2001), Taylor and Stephens (1998), Rossby and Benway (2000), Volkov

(2005) and others have documented an approximately two year lag between the shifts of the Gulf Stream core and NAO events.

Hypothetically, such linkages can be explained by traveling of oceanic perturbations generated by the atmosphere. From the theoretical point of view, Rossby waves significantly affect the large-scale thermohaline ocean circulation and transport across the North Atlantic basin from east to west at speeds of a few cm/s (depending on latitude) (Gill, 1982; Rhines, 2004). It takes months or years to cross the North Atlantic Basin. Several scenarios for ocean wave teleconnections between mid-latitude and tropical Atlantic were proposed in scientific literature (Doscher et al., 1994; Huang et al., 2000; Hakkinen and Mo, 2002; Yang and Joyce, 2003 and others). However, the question of what scenario is of the most importance in transferring decadal signals between the mid-latitude and Tropical Atlantic is still unanswered.

Numerous studies (mostly using results of numerical modeling) demonstrate strong wave variability in the tropics and connections between this variability and large-scale atmospheric perturbations. After analyzing the flow of Antarctic Intermediate Water along the equator in an idealized regional model of the tropical Atlantic Ocean, Jochum and Malanotte-Rizzoli (2003) found that the flow is dominated by the Rossby wave activity related to the annual cycle. Thierry et al. (2004) studied the deep seasonal variability in realistic and simplified GCMs of the equatorial Atlantic Ocean and found that the annual velocity fluctuations are dominated by the lowest odd meridional mode Rossby wave packets. These Rossby waves are generated by the reflection of the directly wind driven, shallow Kelvin wave packets at the eastern boundary. These facts show the importance of the Rossby and Kelvin wave dynamics in the inter-annual variability of mid-latitude Atlantic circulation and in teleconnection (linkage) between tropical and mid-latitude inter-annual variability. Boning and Schott (1993) found deep current fluctuations with magnitude of 5 cm s^{-1} induced by the seasonal cycle of the wind stress and consistent with the long equatorial Rossby waves.

Therefore, the propagation of long baroclinic Rossby waves generated in the eastern North Atlantic in conjunction with the meridional movement of the zero line of wind stress curl

seems to be a reason of the spatial variability along 48°N and a 1-2 years phase lag between NAO and variability of oceanic heat and freshwater transports in mid-latitudes (Brand and Carsten, 2005).

To understand the AMOC variability due to anomalies in surface wind and/or buoyancy forcing, it is necessary to use the planetary wave dynamics with detecting Rossby waves their vertical scales and structure from observations (Liu, 1999; Yang, 2000). The Rossby wave signatures are clearly detected from satellite altimetry [for example, Chelton and Schlax (1996); Osychny and Cornillon (2004)], SST [Cipollini et al. (1997); Hill et al (2000)] and color [Cipollini et al. (2001); Killworth et al. (2004)] in the North Atlantic that allows estimating some propagating features of long baroclinic Rossby waves but not their vertical structure.

At present, observational support for detecting the AMOC variability is quite poor. This is mainly due to lack of three dimensional ocean data (temperature, salinity, velocity) for the entire Atlantic with sufficient temporal and spatial resolution. The lack of data causes less capability in identifying long baroclinic waves in the Atlantic other than satellite observations (Brand and Carsten, 2005) although Rossby wave signal should appear in various ocean fields, such as velocity, temperature, salinity and biological substances at different depths. Following Killworth et al. (2004), baroclinic Rossby waves in the North Atlantic may induce vertical displacements for ocean surface up to 10 cm, for bottom boundary of thermocline up to 50–100 m and for nitrocline up to 10 m. Below the thermohaline, observed large perturbations of temperature and salinity also may be associated with the vertical structure of baroclinic Rossby waves. Thus, it is urgent to produce a quality three dimensional dataset for temperature, salinity, and velocity dataset with sufficient spatial resolution ($1^{\circ} \times 1^{\circ}$) and temporal resolution (1-3 months) for the entire Atlantic for determining the AMOC variability.

3. Detection of MOC below the Ocean Surface

Argo is an internationally coordinated, broad-scale global array of temperature and salinity profiling floats (Fig. 1), and a major component

of the global ocean observing system. There are 3,000 temperature and salinity profiling floats deployed worldwide.



Fig. 1. Argo float (after the website: <http://scrippsnews.ucsd.edu/Releases/?releaseID=696>).

The Global Temperature and Salinity Profile Program (GTSP) is a cooperative international project to develop and maintain a global ocean Temperature-Salinity resource with data that are both up-to-date and of the highest quality. It is a joint World Meteorological Organization (WMO) and Intergovernmental Oceanographic Commission (IOC) project. Functionally, GTSP reports to the Joint Commission on Oceanography and Marine Meteorology (JCOMM), a body sponsored by WMO and IOC and to the IOC's International Oceanographic Data and Information Exchange committee (IODE). GTSP played a key role in the WOCE Upper Ocean Thermal Data Assembly Centre and contributed to the final WOCE Data Resource DVD Version 3. The WOCE was ended in 2002, with some of its activities continuing through a new program, CLimate VARIability (CLIVAR). The GTSP is also recognized by GOOS as an end-to-end data management system for the oceanographic community. Many nations contribute data to the GTSP and without their contributions the project could not exist. Contributions to the data management portion of GTSP are provided by Australia, Canada, France, Germany, Japan and the USA. The quality control procedures used in GTSP were developed by Integrated Science Data Management (ISDM). Readers can find useful information from the following website: <http://www.nodc.noaa.gov/GTSP/overview/aboutGTSP.html>.

The Navy's Master Oceanographic Observational Data Set (MOODS) is a compilation of ocean data observed worldwide consisting of (a) temperature-only profiles; (b)

both temperature and salinity profiles, (c) sound-speed profiles, and (d) surface temperature (drifting buoy). The measurements in the MOODS are, in general, irregular in time and space. Due to the sheer size and constant influx of data to the Naval Oceanographic Office from various sources, quality control is very important. The primary editing procedure included removal of profiles with obviously erroneous location, profiles with large spikes (temperature higher than 35°C and lower than -2°C), and profiles displaying features that do not match the characteristics of surrounding profiles such as profiles showing increase of temperature with depth. The MOODS contains more than 6 million profiles worldwide (Chu, 2006).

4. Detection of MOC above the Ocean Surface

Data collected from satellite altimeter, scatterometer, and SST sensors can be used to detect the MOC and Thermohaline structure. For example, the satellite altimeter (JASON-1, GFO, ENVISAT) and scatterometer data are analyzed and processed into near-real time ocean surface current dataset on 1° × 1° resolution for world oceans (60° S to 60° N), which is posted online as "Ocean Surface Current Analyses - Real Time (OSCAR)". It provides invaluable resources online for various uses include large scale climate diagnostics and prediction, fisheries management and recruitment, monitoring debris drift, larvae drift, oil spills, fronts and eddies, plus opportunities for search and rescue, naval and maritime operations. The methodology for OSCAR combines geostrophic, Ekman and Stommel shear dynamics, and a complementary term from the surface buoyancy gradient. Interested readers are referred to the web site: (www.oscar.noaa.gov/index.html).

5. Optimal Spectral Decomposition (OSD)

The ocean observational data, no matter detected below or above the ocean surface, is usually noisy and sparse. Fig. 2 demonstrates typical observation coverage for two month observation period (October-November, 04). Besides, in some cases major physical characteristics are not explicitly identified by the data. For example, the evident current systems such as Gulf Streams, Kuroshio, ..., are not represented in the OSCAR data.

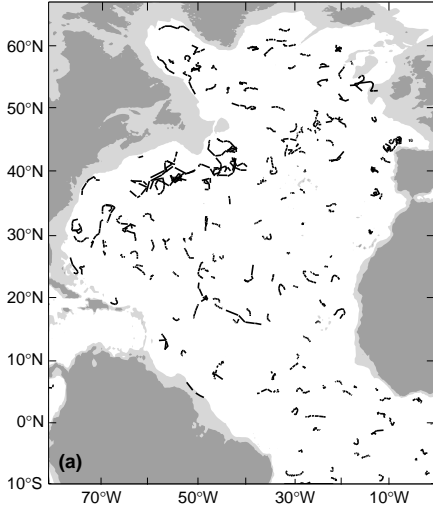


Fig. 2. ARGO subsurface tracks of floats parked at 1000m and 1500m in October-November, 2004 (after Chu et al., 2007).

An optimal spectral decomposition (OSD) method was developed to overcome such weaknesses in ocean observational data. Let velocity \mathbf{U} and temperature T fields be decomposed within the observation period t_{obs} as follows,

$$\begin{aligned}\mathbf{U}(\mathbf{x}, t) &= \bar{\mathbf{U}}(\mathbf{x}) + \tilde{\mathbf{U}}(\mathbf{x}, t) + \hat{\mathbf{U}}(\mathbf{x}, t) + \mathbf{U}'(\mathbf{x}, t), \\ T(\mathbf{x}, t) &= \bar{T}(\mathbf{x}) + \tilde{T}(\mathbf{x}, t) + \hat{T}(\mathbf{x}, t) + T'(\mathbf{x}, t).\end{aligned}\quad (1)$$

Here, $[\bar{\mathbf{U}}(\mathbf{x}), \bar{T}(\mathbf{x})]$ are time averaged velocity and temperature fields; $[\tilde{\mathbf{U}}(\mathbf{x}, t), \tilde{T}(\mathbf{x}, t)]$ represent seasonal variability and dynamical processes with temporal scale, $\tau \leq t_{obs}$; $[\hat{\mathbf{U}}(\mathbf{x}, t), \hat{T}(\mathbf{x}, t)]$ represent faster, mesoscale variability with characteristic temporal scale $\tau \ll t_{obs}$; and $[\mathbf{U}'(\mathbf{x}, t), T'(\mathbf{x}, t)]$ are the measurement noises, $\mathbf{x} = (\varphi, \lambda, z)$ is a right-handed coordinate system with φ the latitude, λ the longitude, and z positive upward.

Our goal is, using irregularly spaced and noisy Argo float observations collected within $\tau_{obs} = 14$ months (between March 2004 and April 2005), to reconstruct

$$\mathbf{U}_{now}(\mathbf{x}_o, t) = \bar{\mathbf{U}}(\mathbf{x}_o) + \tilde{\mathbf{U}}(\mathbf{x}_o, t), \quad (2a)$$

$$T_{now}(\mathbf{x}_o, t) = \bar{T}(\mathbf{x}_o) + \tilde{T}(\mathbf{x}_o, t), \quad (2b)$$

at 1000 m depth, i.e.,

$$\mathbf{x}_o = (\varphi, \lambda, z = -1000 \text{ m}).$$

To reduce measurement errors and noises for velocity calculation, original three-month float

trajectory data are used for the middle month such as March-May 04 for April 04, April-June 04 for May 04, ..., and March-May 05 for April 05. Temperature data are much better because spatial gaps in float coverage are smaller, and the level of noise in the data is lower than for velocity observations. Therefore monthly T-fields are reconstructed in our study. Therefore, hereafter,

$$\begin{aligned}\mathbf{U}_{noise}(\mathbf{x}_o, t) &= \hat{\mathbf{U}}(\mathbf{x}_o, t) + \mathbf{U}'(\mathbf{x}_o, t), \\ T_{noise}(\mathbf{x}, t) &= \hat{T}(\mathbf{x}, t) + T'(\mathbf{x}, t),\end{aligned}\quad (3)$$

are treated as “noise”, which should be removed through the reconstruction process.

Following Eremeev et al. (1993) and Chu et al. (2003a, 2005, 2007) a velocity nowcast $\mathbf{U}_{now}(\mathbf{x}_o, t)$ for quasi-geostrophic currents at any point of the area of interest Ω is written by the form of parameter-weighted sums of the harmonic $Z_i(\mathbf{x}_o)$ and basis $\Psi_k(\mathbf{x}_o)$ functions as

$$\begin{aligned}\mathbf{U}_{now}(\mathbf{x}_o, t) &= \sum_{s=1}^S a_s(t) [\mathbf{k} \times \nabla Z_s(\mathbf{x}_o)] \\ &+ \sum_{k=1}^K b_k(t) [\mathbf{k} \times \nabla \Psi_k(\mathbf{x}_o)].\end{aligned}\quad (4)$$

Similarly, a temperature field is represented by a sum of parameter-weighted basis functions $\Xi_m(\mathbf{x}_o)$ (Chu et al., 2004),

$$T_{now}(\mathbf{x}_o, t) = T_{cl}(\mathbf{x}_o) + \sum_{m=1}^M c_m(t) \Xi_m(\mathbf{x}_o). \quad (5)$$

The spectral coefficients $a_s(t)$, $b_k(t)$, $c_m(t)$ in Eqs. (4) and (5) are functions of time, \mathbf{k} is the vertical unit vector positive upward, $\nabla = (\nabla_\varphi, \nabla_\lambda)$ is the horizontal gradient operator. $T_{cl}(\mathbf{x})$ is the climatic temperature field from World Ocean Atlas (Locarnini et al. 2005).

Where (S, K, M) are the truncated mode numbers.

The harmonic functions $\{Z_i(\mathbf{x}_o)\}$ are the solutions of the horizontal Laplace equation; and the basis functions $\{\Psi_k(\mathbf{x}_o)\}$ $\{\Xi_m(\mathbf{x}_o)\}$ are the solutions of the horizontal Poisson equation with appropriate boundary conditions. Here, we list the equations for determining $\{\Psi_k(\mathbf{x}_o)\}$,

$$\begin{aligned}\nabla_h^2 \Psi_m &= -\lambda_m \Psi_m, \\ \mathbf{n} \cdot \nabla_h \Psi_m |_{\Gamma} &= 0, \\ m &= 1, 2, \dots, M,\end{aligned}\quad (6)$$

where $\Gamma(z)$ is the lateral boundary, $\nabla_h^2 \equiv \partial^2 / \partial x^2 + \partial^2 / \partial y^2$, and \mathbf{n} is the unit vector normal to $\Gamma(z)$. The basis functions $\{\Psi_m\}$ are independent of the data and therefore available prior to the data analysis. The harmonic functions $\{Z_i(\mathbf{x}_o)\}$ are the solutions of the horizontal Laplace equation. After the harmonic functions $\{Z_i(\mathbf{x}_o)\}$ and basis functions $\{\Psi_k(\mathbf{x}_o)\}$ $\{\Xi_m(\mathbf{x}_o)\}$ are given, the Vapnik (1982) variational principle is used to determine the optical spectral truncation (K_{opt} , M_{opt}) in (4) and (5) from a series of velocity (\mathbf{U}_{obs}^p) and temperature (T_{obs}^p) observations at \mathbf{x}_o^p . For the North Atlantic Ocean circulation and thermohaline structure using the Argo/GTSPP data, we find that

$$S = 2, K_{opt} = 20, M_{opt} = 38. \quad (8)$$

The spectral coefficients,

$$\begin{aligned}\mathbf{a} &= [a_1, \dots, a_S]^t, \mathbf{b} = [b_1, \dots, b_{K_{opt}}]^t, \\ \mathbf{c} &= [c_1, \dots, c_{M_{opt}}]^t,\end{aligned}\quad (8)$$

are estimated using an appropriate variation method. Here, the superscript ‘ t ’ shows the transpose operator. The OSD method has two important procedures: optimal mode truncation and determination of spectral coefficients. After the two procedures, the generalized Fourier spectrum (1) is used to provide data at regular grids in space and time. Readers may find detailed description on accuracy of the OSD method from Chu et al. (2007).

6. Mid-Depth North Atlantic Circulation and Thermal Field

6.1. Background

Basin-scale circulations in the North Atlantic are driven by surface winds and heat/freshwater fluxes. The trades (easterlies) and the mid-latitude westerlies are the prevailing winds north of the tropics. They drive the subtropical gyre in the mid-latitude North Atlantic through Ekman convergence and subpolar gyre in the northern side of the westerlies through Ekman divergence.

The subtropical gyre has two western boundary currents - the Gulf Stream (off the east coast of the U.S.) and the North Atlantic Current (off the east coast of Newfoundland/Flemish Cap). The North Atlantic Current makes a major bend offshore at the southern entrance to the Labrador Sea (called the “northwest corner”) and then extends eastward into the mid-Atlantic and then turns northward into the subpolar region as the Subarctic Front. The subtropical gyre also has an eastern boundary current called the Canary Current. The wind-driven subtropical gyre is largely gone by about 2000 m depth.

The deep-water formation in the Labrador and Nordic seas drives the Meridional Overturning Circulation (MOC). It transports cold deep water southward mainly by the Deep Western Boundary Current (DWBC), and transports warm surface water northward from the southern Atlantic Ocean by the cross-equatorial currents. Changes in the Labrador Cold water formation affect the MOC and subsequently the sea surface temperature (SST) in the tropics, and in turn affect the climate change.

There is much evidence that the dominant mode of the low-frequency atmospheric variability in the North Atlantic, the North Atlantic Oscillation (NAO), affects the Labrador Cold Water (LCW) formation and ocean heat transport variability. For example, during the World Ocean Circulation Experiment (WOCE) from 1990 to 1998 nine realizations of the so-called “48°N” section along the line between the English Channel and the Grand Banks of Newfoundland showed significant inter-annual changes in the climate for relevant key parameters of the large-scale circulation in the North Atlantic, such as heat and fresh water transports. With a phase lag of 1-2 years, the transports are near-linearly correlated to the change of the NAO index [Bersh, 2002]. Frankignoul et al. [2001], Taylor and Stephens [1998], Rossby and Benway [2000], and Volkov [2005] have documented an approximately 2 year lag between the shifts of the Gulf Stream core and the NAO events.

Although the North Atlantic is a subject of intensive theoretical and observational studies for many years, quantitative description on the large-scale mid-depth circulation and thermal field especially the temporal variability is quite limited. There are several attempts to construct the large-scale mid-depth circulation pattern for regional seas in the North Atlantic with higher

resolution using subsurface float (SOFAR, RAFOS, ALACE, PALACE, SOLO) trajectories directly or combining with hydrological observations [Lavender et al., 2000; 2005; Zhang et al., 2001; Bower et al., 2002; Kwon and Riser 2005] but for the whole North Atlantic using climate data [Schmitz and McCartney, 1993; Reid, 1994; Chu, 1995; Lozier et al., 1995].

The Argo float data are used to determine the spatial-temporal structure of the basin-scale circulation and thermal field in the North Atlantic basin (4°N-65°N) at mid-depth (1000 m), to estimate the eddy kinematical characteristics of the circulations, and to calculate the horizontal heat flux. To do so, the recently developed OSD method is used. Our results are not inconsistent with the bulk of the earlier studies, but the results presented here have better spatial and temporal coverage than most previous studies. The mid-depth (1000 m depth) currents and temperature were reconstructed with the same spatial resolution of $1^\circ \times 1^\circ$ in the whole North Atlantic excluding the near-equatorial area south of 4°N.

6.2. Circulations

The mid-depth mean velocity (April 2004 to March 2005) can be calculated from the Argo float track data using the bin technique. The arrows are the mean velocities averaged over appropriate ($4^\circ \times 4^\circ$) bins. The circulation patterns, robust to variations of bin sizes, show well-known circulation features identified from early analyses on the RAFOS float trajectories in separate regions of the North Atlantic.

The measurement cycle of an Argo profiling float includes four stages: ascending, surface drifting, diving and deep drifting. The Argo float can only get its position fixings while it ascends to the sea surface. The vector between two consecutive surface positions during the deep drifting divided by the time interval is taken as the mid-depth velocity vector. When the Argo float is diving, ascending and drifting below the sea surface, no data can be transmitted to the ground stations in real time. Velocity field after the first step analysis shows noisy circulation patterns (Figs. 2 a, b) with large spatial gaps (from 230 km to 800 km).

Uncertainty in the Argo float data causes errors in the velocity field. First, the data extracted from the floats parking at two different levels:

1000 m and 1500 m and grouped together to represent the mid-depth (1000 m). This neglects the vertical shear. Second, the vertical shear causes increase or decrease of the distance between the points of ascending from and diving to the parking depth. Third, the sequence of float trajectory segments only approximates the real Lagrangian paths. Fourth, preliminary computations (not included here to be published in a separate paper) show that high resolution elements of circulation in the western North Atlantic, such as the northern re-circulation gyre and the Deep Western Boundary Current (DWBC) are also revealed by the Argo floats. For example Fig 3 clearly shows the existence of DWBC. However, such a resolution is not available for the whole North Atlantic. The high-energetic mesoscale eddies and narrow boundary currents are classified as “noise” and removed from the analysis. Fifth, there are large spatial gaps in Argo float trajectories. The boundary consists of three segments: Γ_1 and Γ_2 approximate the 1000 m isobath and the Azores Plateau; Γ_3 is an open boundary along 4°N latitude. This domain is extended to 10°S (Γ_3') with zero tangential velocity and diffusion flux.

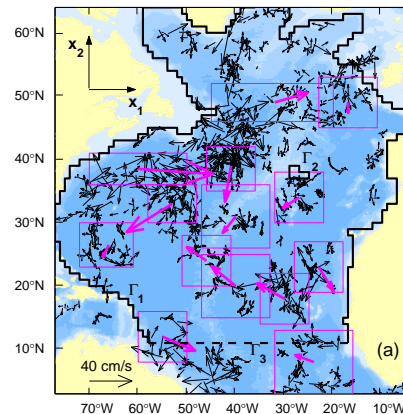


Fig.3. Circulation velocities (tiny arrows) estimated from the original ARGO float tracks at 1000 m for Dec 2003–Mar 2004. The figure scale is given for tiny arrows. Red arrows are circulation velocities obtained by averaged over appropriate bins (red lines). The magnitude of these arrows are multiplied by scale equaled to 20 for better visualization of schematic circulation patterns. Γ_1 , Γ_2 and Γ_3 are boundaries of the computation area.

The reconstructed annual mean circulation (April 2004 – March 2005) is characterized by four major gyres (Fig. 4): tropical double gyres (south of 20°N), anticyclonic subtropical gyre (20°N to about 50°N), and cyclonic subpolar gyre (North of 50°N).

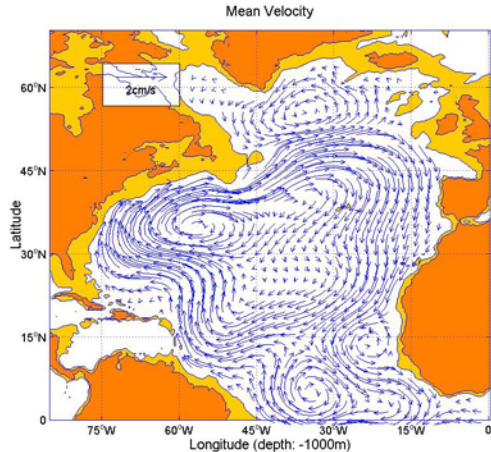


Fig. 4. Mean circulation at 1000 m depth from April 2004 to March 2005 computed using the OSD method.

6.2.1. Tropical Gyre

The tropical gyre is an elongated cyclonic gyre with velocities in a core of less than 2 cm/s and does not correspond to the schematic flow diagram for 500 to 1200 m proposed by Stramma and Schott [1999] (see, also, Schmid et al. 2005). However, a spatial pattern corresponding to a cyclonic flow approximately around the center of Guinea dome (12°N, 22°W) is clearly seen in Fig. 4. That agrees, for example, with El Moussaoui et al. (2005) who observed the quasi-permanent cyclonic flow of the Guinea dome at the same depth and deeper.

Seasonal evolution of the circulation in 2004 (Fig. 5) indicates a superposition of eddy-wave-like perturbations (mainly cyclonic rotation) propagating northwestward, and westward from the eastern Tropical North Atlantic. These perturbations affect the mid-depth flow along the African coast and probably the Intermediate Western Boundary Current (IWBC). That results in seasonal reversals for boundary currents. The currents are northwest near the African coast up to 16°N in January 2004 (Fig. 5a) with a maximum speed of about 3 cm/s. As the cyclonic eddy propagated northwestward, the currents reversed to southward and southwestward in April, changed southward in April 2004 (Fig. 5b), and reversed the direction

again to southeastward in October 2004 (Fig. 5d). Evidences for this result also can be found in El Moussaoui et al [2005], Fratantoni and Richardson [1999] and others. Clearly, the reconstructed fields have too lower resolution to be used for the analysis of narrow boundary currents, such as IWBC. Therefore, fall-winter reversals of IWBC from northwestward to southeastward which may be observed south of 15°N [Stramma and Schott, 1999], are not explicitly extracted from our results. However, Chu et al. (2007) found the Rossby wave propagation in the tropical North Atlantic using the same ARGO track data.

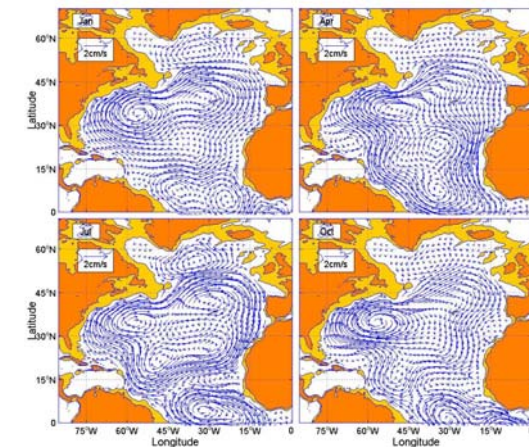


Fig. 5. Evolution of circulation at 1000 m depth in 2004 for (a) January, (b) April, (c) July, and (d) October 2004.

6.2.2. Subtropical Gyre

The North Atlantic subtropical gyre includes the Gulf Stream, which becomes the North Atlantic Current at about 40° N and 45°W and flows northeasterly across the North Atlantic. It recirculates at the west coast of England and splits into southwestward flowing current along the mid-ocean range and the southward flowing Canary Current along the west coast of Spain, Portugal, and North Africa. The mean Canary Current is weak at 1000 m depth and merges with the North Atlantic Equatorial Current, thus completing the North Atlantic subtropical gyre (Fig. 5). The subtropical gyre contains three evident cyclonic eddies with the west one. The subtropical gyre has evident temporal variation at 1000 m depth.

6.2.3. Subpolar Gyre

The subpolar gyre of the North Atlantic is a region of complex dynamics, playing a key role in the variability of climate. Its currents are

forced by buoyancy contrasts and overflows from neighboring seas, probably as much as by the wind. Because of the low stratification, topography steers the currents, even in the upper layers. The different water masses, although well defined by the precision of hydrographic measurements, have salinity contrasts small enough that numerical models have difficulty to maintain them.

Fig. 5 shows that the fastest flows are along the northern and western boundaries of the basin and near Flemish Cap, including the subsurface signature of the northward-flowing North Atlantic Current. Flow around the Reykjanes Ridge and the local acceleration through the Charlie Gibbs Fracture Zone illustrate apparent topographic control, while reversing zonal flows exist just north of the Azores Plateau.

6.3. Temperature Field

The mid-depth annual mean temperature field (April 2004 to March 2005) can be calculated from the Argo profiling data using the OSD technique (Fig. 6). The thermal field shows well-known features identified from early analyses on the World Ocean Atlas for the North Atlantic. The annual mean temperature field from April 2004 to March 2005 identified from the Argo profiling data is quite similar to the climatological mean temperature field except a cold eddy occurs in the western tropical North Atlantic (10°–20°N) with the temperature cooler than 5°C.

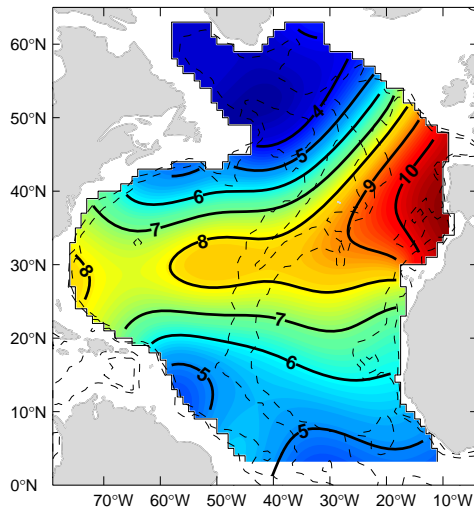


Fig. 6. Annual mean temperature fields at 1000 m depth computed from the ARGO profile data (April 2004 to March 2005).

Temporal evolution of the temperature field at mid-depth shows a warm zone appears in the mid-latitudes with around 8°C in the western North Atlantic (23°N - 35°N) and around 10°C in the eastern North Atlantic (30° N-50°N). This warm zone is sandwiched by two cold zones with 5°C – 6°C in the tropical one, and colder than 4°C in the polar one. The most evident feature is the formation of a warm eddy in the western mid-latitudes. This eddy was formed in December 2004 and sustained until February 2005.

6.4. Error Statistics

The reconstructed monthly temperature field T_{now} is evaluated at regular grid points. We interpolate T_{now} to the observational points for that month and compute the residuals,

$$T' = T_{obs} - T_{now}. \quad (7)$$

To show the statistical characteristics of T' , the North Atlantic is divided into 4 presumably dynamically different sub-basins: tropical region, western mid-latitudes, eastern mid-latitudes, and polar region. The error histograms of T' (Fig. 7) show non-Gaussian distribution since the kurtosis is much higher than 3. The error standard deviation is around 0.6°C. The error T' is positively skewed with skewness ranging from 0.86 to 1.00. The bias (mean T') is quite small from 0.05°C to 0.07°C.

6.5. Mid-Depth Long Baroclinic Rossby Waves

Identification of long Rossby wave of tropical North Atlantic at mid-depth (~1000 m) from the Argo track data is taken as an example to demonstrate the usefulness of the OSD method to reanalyze sparse and noisy ocean data (Chu et al., 2007). Argo float data (subsurface tracks and temperature profiles collected from March, 04 through May, 05) are used to detect signatures of long Rossby waves in velocity of the currents at 1000 m depth and temperature, between the ocean surface and 950 m, in the zonal band of 4°N -24°N in the Tropical North Atlantic. Different types of long Rossby waves (with the characteristic scales between 1000 km and 2500 km) are identified in the western [west of the Mid-Atlantic Ridge (MAR)] and eastern [east of the MAR] sub-basins.

Current velocities computed along the original (non-smoothed) Argo tracks in November-

December, 2004 are shown in Fig. 7 as red arrows.

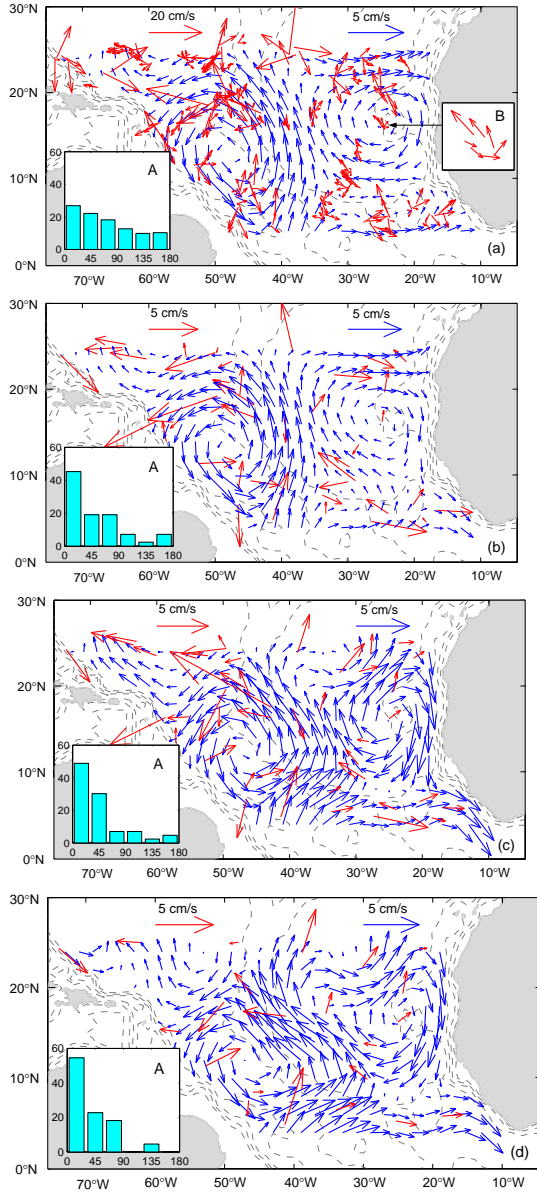


Fig. 7. Sensitivity of the reconstructed circulation patterns to filtration of the original data: OSD is applied to (a) the original data (November-December, 04); (b) the original data (November-December, 04) filtered with a 2-month window; (c) the original data (October-December, 04) filtered with a 3-month window; (d) the original data (October-December, 04) filtered by $4^\circ \times 4^\circ$ bin averaging; Blue and red arrows correspond to the reconstructed circulation and original/filtered data. For α -histograms (inserts A) the x-axes is the angle α and the y-axis is the number of comparisons (%), as described in subsection 4.3 (after Chu et al., 2007).

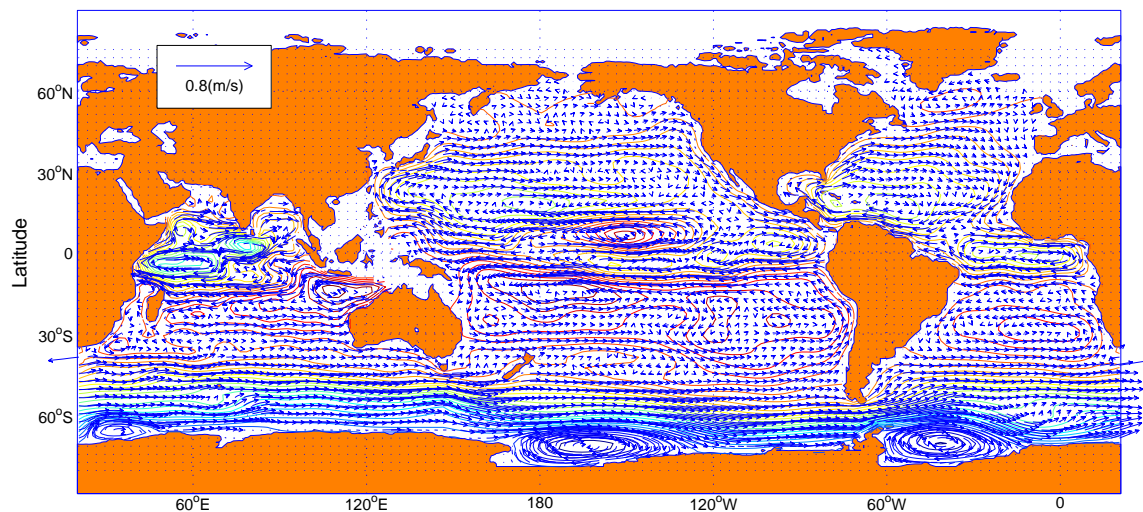
A strong contribution from intensive eddies, such as that shown in inset B, narrow jets and measurement errors is clearly identified here. Visually, the velocity pattern corresponding to the original data looks quite chaotic, and there are 500-600 km spatial gaps in observation coverage. To understand the reconstruction skill for such data we applied three criteria: (1) the formal mean square error (the reconstruction error) computed by the “laminar ensemble” technique (Turchin et al., 1971), (2) statistics of angle (α) between the reconstructed and observed velocity at float locations, and (3) stability degree of the reconstructed snapshot on observation sampling (Perry and Chong, 1987).

7. Converting Idealized Currents into Realistic Currents

Near-real time ocean surface currents derived from satellite altimeter (JASON-1, GFO, ENVISAT) and scatterometer data on $1^\circ \times 1^\circ$ resolution for world oceans (59.5° S to 59.5° N) posted online as “Ocean Surface Current Analyses – Real Time (OSCAR)”, provide invaluable resources online for various uses include large scale climate diagnostics and prediction, fisheries management and recruitment, monitoring debris drift, larvae drift, oil spills, fronts and eddies, plus opportunities for search and rescue, naval and maritime operations. The methodology for OSCAR combines geostrophic, Ekman and Stommel shear dynamics, and a complementary term from the surface buoyancy gradient.

A major weakness of the OSCAR dataset is its inability to represent the currents near the lateral boundary. The most evident western boundary currents such as the Gulf Stream and Kuroshio are missing (Fig. 7b). The OSD method is used to reconstruct the OSCAR data. After the OSD analysis, the reconstructed OSCAR data show realistic surface circulations including western boundary currents such as Gulf stream, Kuroshio, Brazilian Currents, Somali Currents, and eastern boundary currents such as California Currents, Peru Currents, etc. (Fig. 7a).

With the establishment of 4D (time and space) synoptic temperature, salinity, and velocity (STSV) data, the MOC/ thermohaline structure as well as their variability can be effectively identified.



Original Data 2007 Jun 15

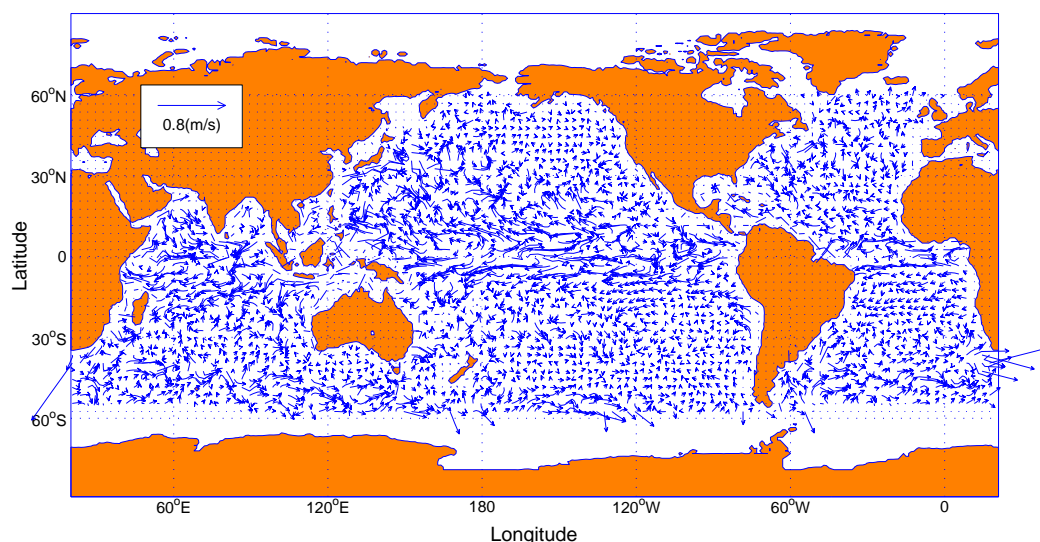


Fig. 7. Ocean surface currents on 15 June 2007: (a) after the OSD analysis, and (b) from original OSCAR data.

8. Conclusions

Our main objective is to provide the scientific and operational communities with three-dimensional ocean fields (temperature, salinity, and velocity) that have higher resolutions and better coverage than any products available. With our unique access to the baseline GTSP-Argo, OSCAR, and Navy's MOODS data, our strong experience with the data processing, and our established near-real-time and online data distribution system in NODC, we plan to produce and distribute this 3D synoptic temperature, salinity, and velocity (STSV),

which will be primarily based on the GTSP-Argo, OSCAR, and Navy's MOODS data. A more flexible and user-driven data processing and distributing system will be implemented, to optimize data use by both the scientific and operational communities.

With 3D STSV data, temporal (seasonal and inter-annual) and spatial (various scales) variability of AMOC can be identified through quantifying the derived variables such as the meridional overturning (MO) streamfunction, heat storage, meridional heat transport, etc.. The physical mechanisms causing the AMOC variability can be determined through correlation

analysis between the STSV data (including derived variables) and surface atmospheric data or investigation of the role of long baroclinic Rossby waves (longer than 500 km) generated in the eastern Atlantic on the AMOC variability.

The impact of the AMOC variability on rapid climate change can be evaluated through the correlation analysis between STSV data the large-scale atmospheric variability (characterized by NAO).

With the gridded STSV data, we are analyzing the variability and structure of the AMOC and explore the mechanisms contributing to AMOC variability using the new 3D STSV data together with the NCEP surface atmospheric data. We plan to work closely with the Naval Oceanographic Office and NOAA/NCEP to apply the STSV data for quantitative assessment on the AMOC variability and operational monitoring of the AMOC variability and in turn the rapid climate change.

Acknowledgments

NOAA, NODC, ONR, and the Naval Oceanographic Office sponsored this research.

References

Bersh, M., 2002: North Atlantic oscillation-induced changes of the upper layer circulation in the northern North Atlantic Ocean. *J. Geophys. Res.*, 107, C10, 20-1–20-11.

Boning, C.W., and F.A. Schott, 1993: Deep currents and the eastward salinity tongue in the equatorial Atlantic: results from an eddy-resolving, primitive equation model. *J. Geophys. Res.*, 98 (C4), 6991-6999.

Boning C.W. and J. Kroger, 2005: seasonal variability of deep currents in the equatorial Atlantic: a model study. *Deep-Sea Research*, I, 52, 99-121.

Brandt, P., and C. Eden, 2005: Annual cycle and inter-annual variability of the mid-depth tropical Atlantic Ocean. *Deep-Sea Research I*, 52, 199-219.

Broecker, W.S., 1997: Thermohaline circulation, the Achilles's heel of our climate system: Will man-made CO₂ upset the current balance? *Science*, 278, 1582-1588.

Chelton, D.B., and M.G. Schlax, 1996: Global observations of oceanic Rossby waves. *Science*, 272, 234-238.

Chu, P.C., L.M. Ivanov, T.M. Margolina and O.V. Melnichenko, 2002: On probabilistic stability of an atmospheric model to differently scaled perturbations, *J. Atm. Sci.*, 59, 19, 2860–2873.

Chu, P.C., L.M. Ivanov, T.M. Margolina, T.P. Korzhova, and O.V. Melnichenko, 2003a: Analysis of sparse and noisy ocean current data using flow decomposition. I. Theory, *J. Atmos Oceanic Tech.*, 20, 478 - 491.

Chu, P.C., Ivanov, L.M., Margolina, T.M., Korzhova, T.P., and O.V. Melnichenko, 2003b: Analysis of sparse and noisy ocean current data using flow decomposition. Part 2. Applications to Eulerian and Lagrangian data. *J. Atmos. Oceanic Tech.*, 20, 492–512.

Chu, P.C., L.M. Ivanov, and T.M. Margolina, 2004: Rotation method for reconstructing process and fields from imperfect data. *Int. J. Bifur. Chaos*, 14 (8), 2991-2997.

Chu, P.C., L.M. Ivanov, O.V. Melnichenko, 2005 a: Fall-Winter Current Reversals on the Texas-Louisiana continental shelf. *J. Phys. Oceanog.*, 35, 902-910.

Chu, P.C., L.M. Ivanov, and T.M. Margolina, 2005 b: Seasonal Variability of the Black sea chlorophyll-a. *J. Mar. Sys.*, 56, 243-261.

Chu, P.C., L.M. Ivanov, O.V. Melnichenko, and N.C. Wells, 2007: On long baroclinic Rossby waves in the tropical North Atlantic observed from profiling floats. *Journal of Geophysical Research*, 112, C05032, doi:10.1029/2006JC003698.

Cipollini P., D. Cromwell, M. S. Jones, G.D. Quartly and P.G. Challenor, 1997: concurrent altimeter and infrared observations of Rossby wave propagation near 34°N in the Northeast Atlantic, *Geophys. Res. Lett.*, 24, 8, 8889-892.

Cipollini, P., D. Cromwell, P.G. Chanselor and S. Raffago, 2001: Rossby waves detected in global ocean color data, *Geophys. Res. Lett.*, 28, 2, 323-326.

Curry, R.G. and McCartney, 1996: Labrador Sea Water carries northern climate signal south. *Oceanus*, 39, 24-28.

Curry R.G., M.S. McCartney and T.M. Joyce, 1998: Oceanic transport of subpolar climate signals to mid-depth subtropical waters. *Nature*, v. 391, 5, 575-577.

Doscher, R., C.W. Boning and P. Herrmann, 1994: Response of Circulation and heat transport in the North Atlantic to changes in thermohaline forcing in northern latitudes: a model study. *J. Phys. Ocean.*, 24, 11, 2306-2320.

- Emery, W.J., and R.E. Thompson, 1998: Data analysis methods in physical oceanography. Pergamon, New York, 634 pp.
- Enomoto, T., and Y. Matsuda, 1999: Rossby wave packet propagation in a zonally-varying basic flow. *Tellus*, 51A, 588-602.
- Gill, A.E., 1982: Atmosphere-ocean Dynamics, Academic Press, San Diego.
- Frankignoul, C., G. de Coetlogon, T.M. Joyce, and S. Dong, 2001: Gulf Stream variability and ocean-atmosphere interactions. *J. Geophys. Res.*, 31, 3516-2359.
- Hakkinen S., and K.C. Mo, 2002: The low-frequency variability of the Tropical Atlantic Ocean. *J. Climate*, 15, 3, 84-93.
- Hill, K.L., I.S. Robinson, and P. Cipollini, 2000: Propagation characteristics of extra-tropical planetary waves observed in the ATSR global sea surface temperature record. *J. Geophys. Res.*, 105, C9, 21,927-21.945.
- Huang, R.X., M.A. Cane, N. Naik, and P. Goodman, 2000: Global adjustment of the thermocline in response to deep-water formation. *Geophys. Res. Lett.*, 27, 6, 759-762.
- Hurrell, J.W., and K.E. Trenberth, 1999: Global sea surface temperature analyses: multiple problems and their implications for climate analysis, modeling and reanalysis. *Bull. Amer. Meteor. Soc.*, 80, 2661-2678.
- Ivanov, L.M., A.D. Kirwan, Jr., and T.M. Margolina, 2001: Filtering noise from oceanographic data with some applications for the Kara and Black Seas. *J. Mar. Sys.*, 28, 1-2, 113-139.
- Killworth P.D., P. Cipollini, B. Mete Uz, and J. R. Blundell, 2004: Physical and biological mechanisms for planetary waves observed in satellite-derived chlorophyll. *J. Geophys. Res.*, C07002, 1-18.
- Large, W.C., and A.J. Nurser, 2001: Ocean surface water mass transformation. Ocean Circulation and Climate, G. Siedler et al., Eds., International Geophysics series, v. 77, Academic Press, 317-336.
- Liu Z., 1999: Forced planetary wave response in a thermohaline gyre. *J. Phys. Ocean.*, 29, 1036-1055.
- Lorenz, E.N. 1984: Irregularity. A fundamental property of the atmosphere. *Tellus*, 42,98-110.
- Lumpkin, R., and K. Speer, 2003: Large-scale vertical and horizontal circulation in the North Atlantic. *J. Phys. Ocean.*, 33, 9, 1902-1920.
- McWilliams, J.C., N.J. Norton, P. Gent and D. B. Haidvogel, 1990: A linear balance model of wind-driven, mid-latitude ocean circulation. *J. Phys. Ocean.*, 20, 9, 1349-1378.
- Mundt, M.D., G.K. Vallis, and J. Wang, 1997: Balanced Models and dynamics for the large- and mesoscale circulation. *J. Phys. Oceanogr.*, 27, 6,1133-1152.
- Osychny V., and P. Cornillon, 2004: Properties of Rossby Waves in the North Atlantic Estimated from Satellite Data. *J. Phys. Oceanogr.*, 34,1, 61-76.
- Polito P.S., and P. Cornillon, 1997: Long baroclinic Rossby waves detected by TOPEX/POSEIDON. *J. Geophys. Res.*, 102, C2, 3215-3235.
- Rhines P., 2004: Oceanic and atmospheric Rossby waves. A lecture for the Norman Phillips symposium at the annual Amer. Meteorological Society meeting (available from the website: <http://www.ocean.washington.edu/research/gfd/papers-rhines.html>).
- Roebber, P.J. 1995: Climate variability in a low-order coupled atmosphere-ocean model. *Tellus*, 47A, 473-494.
- Rossby, T., and R.L. Benway, 2000: Slow variations in mean path of the Gulf Stream east of Cape Hatteras. *Geophys. Res. Lett.*, 27, 117-120.
- Susanto, R. D., Q. Zheng, and X.-H. Yan, 1998: Complex singular decomposition analysis of equatorial waves in the Pacific observed by TOPEX/POSEIDON altimeter. *J. Atm. Ocean. Tech.*, 15, 3, 764-774.
- Taylor, A.H., and J.A. Stephens, 1998: The North Atlantic Oscillation and the latitude of the Gulf Stream. *Tellus*, 50A, 134-142.
- Thiebaux H.J., and M.A. Pedder, 1987: Spatial Objective Analysis: with Applications in Atmospheric Science. Academic Press, 299 pp., London.
- Thierry, V., A.M. Treguer, and H. Mercier, 2004: Numerical study of the annual and semi-annual fluctuations in the deep equatorial Atlantic Ocean. *Ocean Modelling*, 6, 1-30.
- Vapnik, V.N., 1982: Estimation of Dependencies Based on Empirical Data. Springer-Verlag, 379 pp., New York.
- Volkov D.L., 2005: Interannual variability of the altimetry-derived eddy field and surface circulation in the extra-tropical North Atlantic Ocean in 1993-2001. *J. Phys. Oceanogr.*, 35, 4, 405-426.
- Walín, G., 1982: On the relation between sea-surface heat flow and thermal circulation in the ocean. *Tellus*, 34, 187-195.

Yang, J., 1999: A linkage between decadal climate variations in the Labrador sea and the Tropical Atlantic Ocean. *Geophys. Res. Lett.*, v. 26, 8, p. 1023-1026.

Yang H., 2000: Evolution of long planetary wave packets in a continuously stratified ocean. *J. Phys. Oceanogr.*, 30, 2111-2123.

Yang, J., and T.M. Joyce, 2003: How do high-latitude North Atlantic climate signals the crossover between the deep Western Boundary Current and the Gulf Stream? *Geophys. Res. Lett.*, 30, 2, 42-1 - 42-4.